frontiers | Frontiers in Soil Science

TYPE Original Research
PUBLISHED 25 February 2025
DOI 10.3389/fsoil.2025.1540941

OPEN ACCESS

EDITED BY
Prafulla Kumar Sahoo,
Central University of Punjab, India

REVIEWED BY
Sivakumar Karthikeyan,
Alagappa University, India
Tofan Kumar Rout,
Central Drug Research Institute (CSIR), India
Maulana Arif,
Andalas University, Indonesia

*CORRESPONDENCE
Xiaoxue Wang
2503613509@qq.com
Yujiao Liu
Liuyj@mail.crsri.cn

RECEIVED 18 December 2024
ACCEPTED 03 February 2025
PUBLISHED 25 February 2025

CITATION
Li Z, Wang X, Liu Y, Li W, Zhou X, Lv C, Wang G and Ma J (2025) Comprehensive analysis of sediment grain features and their engineering implications in the Yangtze River source area. *Front. Soil Sci.* 5:1540941. doi: 10.3389/fsoil.2025.1540941

Comprehensive analysis of sediment grain features and their engineering implications in the Yangtze River source area

Zhijing Li[1,2], Xiaoxue Wang[1,2]*, Yujiao Liu[1,2,3]*, Wenqi Li[1,2], Xian Zhou[1], Chaonan Lv[4], Guiqiao Wang[5] and Junxiao Ma[1,2]

[1]Changjiang River Scientiffc Research Institute of Changjiang Water Resources Commission, Wuhan, China, [2]Key Laboratory of River Regulation and Flood Control in Middle and Lower Reaches of Yangtze River of Ministry of Water Resources, Wuhan, China, [3]State Key Laboratory of Hydraulics and Mountain River Engineering, Sichuan University, Chengdu, China, [4]China Three Gorges Corporation, Yichang, China, [5]College of Water Conservancy and Hydropower Engineering, Hohai University, Nanjing, China

Introduction: The particle size characteristics of irregular sediments in the Yangtze River Source Area (YRSA) are pivotal for understanding the mechanical properties of the sedimentary medium.

Methods: This study utilizes field sediment sampling, laser scanning, laboratory testing, and mathematical statistics to analyze the morphological, geometric, mineralogical, and accumulation characteristics of sediment particles in the region.

Results: Our findings indicate that sediments in the YRSA have angular edges and deviate from spherical shapes, exhibiting elongated and flatter three-dimensional morphologies. In the experiment, the sliding plate method was used to measure the angle of repose of the sediments, which was found to be 36.7° above water and 35.9° below water. Both values are higher than the typical range for non-plateau regions, indicating reduced sediment mobility. The sediments are composed of fine-grained and coarse-grained soils. The particle size distribution is primarily coarse sand (0.5-2.0 mm), fine gravel (2.0-5.0 mm), and medium gravel (5.0-20.0 mm), with a significant coarsening trend observed over the past six years. The mineral composition, dominated by quartz, feldspar, and heavy minerals, is stable, with approximately 70% of the minerals having a hardness of $\geq$ 7 on the Mohs scale. The most abundant trace elements are Ti, Mn, Ba, P, Sr, Zr, and Cl.

Discussion: This research reveals that the sediment characteristics in the YRSA are markedly different from those of natural sands in non-plateau regions, necessitating a reevaluation of conventional theories and engineering practices for engineering constructions in this area. The insights from this study are profound and practically relevant, illuminating the sediment transport dynamics in alpine river systems and supporting sustainable regional development.

KEYWORDS

Yangtze River source area, sediment characteristics, geometric characteristics, particle size distribution, accumulation state, mineral composition

1 Introduction

Global warming, a preeminent environmental issue of the contemporary era, exerts profound and extensive implications (1–5). It has significantly perturbed the hydrological cycle, leading to a marked increase in the frequency and intensity of extreme precipitation and runoff events (2, 6). The alteration in runoff volume not only directly modifies the spatial distribution and availability of water resources but also substantially impacts sediment transport processes in rivers. The YRSA, located at the heart of the Tibetan Plateau with 78% of its area underlain by permafrost (7), is particularly vulnerable. The Yangtze River, the longest in Asia, has distinct reaches with unique geomorphological and hydrological features. Channel bars, point bars, and riverbeds are key depositional landforms that influence navigation, flood control, and ecosystem health (8). Climate warming has intensified the water and sediment flux in this region, resulting in more pronounced braided river structures, lateral expansion, and severe bank erosion and retreat, thereby undermining the stability of riverbeds (9–11). Concurrently, the escalation in temperatures has markedly diminished the stability of glacial till (12, 13), altered the geochemical indicators of sediments (14), and triggered novel soil erosion phenomena, such as thermokarst slumping (15–17). This cascade of effects is not merely associated with the natural evolution of river landforms but also profoundly disrupts the equilibrium of river ecosystems. Moreover, it poses a significant threat to the sustainability of human socio-economic activities, including reservoir functionality, agricultural irrigation, urban water supply, navigation transport, and flood control (18, 19).

Sediment transport is an exceedingly intricate and multifactorial natural process, fundamentally hinged on how the physicochemical attributes of sediment govern its behavioral patterns within water currents. These attributes, encompassing particle size, shape, density, porosity, and chemical properties (20–23), act in concert to modulate the processes of sediment suspension, transport, and deposition. In-depth investigations into the properties of sediment are crucial for enhancing our understanding of sediment transport mechanisms (24, 25), soil erosion control (26), river channel evolution prediction (27), and reservoir sedimentation management (28).

Investigations into the properties of sediment have evolved into a multidisciplinary pursuit (27, 29–33), leveraging sophisticated technologies such as remote sensing, high-speed photography, and dynamic image analysis (34–36) for both experimental modeling and numerical simulations (37, 38). Visher's Plot (39), which identifies sub-populations within individual log-normal grain size distributions, has been effectively utilized in numerous sedimentological investigations to elucidate depositional environments and sedimentary processes. Previous research has elucidated that the bulk density and porosity of sediment modulate inter-particle cohesive forces, thereby influencing the compaction and transport dynamics of sediment deposition (40, 41). Notably, the morphology of particles exerts a more pronounced effect on sediment transport than their density, and the integration of shape factors into predictive models substantially enhances the accuracy of sediment transport capacity forecasts (42). Modifications in the composition of bed sediment significantly alter the characteristics of sediment transport rates. The gradation of sediment dictates its suspension and conveyance capabilities within water currents, which is pivotal for the settling attributes of sediment (43, 44). For instance, under optimal mixing ratios, the transport efficiency of non-uniform bed loads exceeds that of uniform bed loads of equivalent size (45). The concentration and size distribution of suspended sediment govern its suspension and settling behaviors, which in turn have a substantial impact on processes of riverbed erosion and sedimentation (22, 46). Furthermore, the abundance and distribution of geochemical elements are markedly contingent upon the grain size of sediment (43). The sedimentary environmental shifts in the Eastern Yangtze Block have precipitated corresponding alterations in sediment composition and structure, characterized by an ascending siliceous fraction and conspicuous variations in the carbonate fraction (47). Spatially, the physical and chemical attributes of sediment exhibit a discernible pattern of variation, which is profoundly modulated by hydrodynamic conditions, thereby sculpting the particle sorting and grain size characteristics of sediment. In the inner estuary of the Yangtze River, sediment is predominantly composed of fine-grained constituents (clay and silt), predisposed to settle in locales with diminished hydrodynamic activity. In contrast, nearshore sediments generally possess larger grain sizes, primarily composed of fine sand and gravel (48).

Although studies have made strides in understanding sediment particle characteristics, the harsh climate and scarcity of field measurement data in the YRSA have impeded a comprehensive understanding of sediment properties. To bridge this research gap, our study investigates the physical and chemical properties of sediments from the YRSA and compares them with those from non-source areas to better understand the characteristics of sediment in alpine rivers. The findings from this study provide a foundation for comprehending sediment movement patterns, evaluating riverbed morphological changes, informing related engineering constructions, and devising ecological protection strategies. Additionally, a profound understanding of the fundamental characteristics of sediment movement is essential for flood safety construction, reducing climate change risks, and fostering regional sustainable development.

2 Materials and methods

2.1 Study area

The YRSA, as the upstream core region monitored by the Zhidamen Hydrological Station, is essential within the Sanjiangyuan Nature Reserve and plays a crucial role in the natural evolution and ecological protection of the Yangtze River Basin. Located in the hinterland of the Qinghai-Tibet Plateau, this area extends from 32°30′N to 35°40′N and 90°30′E to 94°00′E, covering 140,000 square kilometers with an average altitude of 4,000 meters and exhibiting a distinctive plateau topography. The terrain, which descends from higher elevations in the west to lower in the east, is marked by continuous and steep gradients, as well as the extensive development of braided river systems (49). This

10.3389/fsoil.2025.1540941

geography creates a complex dynamic environment conducive to the study of river erosion, transportation, and sediment deposition, highlighting its significance for understanding the sediment characteristics of the Yangtze River Basin. A visual representation of the study area is provided in Figure 1.

2.2 Sample collection

Between April 12 and 24, 2023, a comprehensive sampling campaign was conducted within a 10-km-radius area of the Tuotuo River Bridge (92°44′E, 34°22′N) in Tanggula Mountain Town, Qinghai Province. A total of 200 sediment samples were collected from river islands, point bars, and the riverbed. The sampling location is shown in Figure 2. The sampling protocol mandated careful excavation to a depth of 20 centimeters to maintain the integrity of the underlying sediment layers. The samples were promptly transferred to sterile containers, sealed, and meticulously labeled with detailed metadata, including the collection time, geographic coordinates, depth, and environmental conditions. Following drying and weighing, the samples underwent digital imaging to facilitate the analysis of sediment particle morphology and the examination of their morphological characteristics.

2.3 Processing method

2.3.1 Particle morphological characteristics

In light of the characteristics observed in fine sediment particle images acquired through scanning electron microscopy, we utilized our self-developed "Software for Geometric Morphological Analysis and Calculation of Sediment Particles Based on Dynamic Image Recognition V1.0" to determine the morphological parameters of these particles. Initially, digital microscopic cameras were employed to capture images of sediment particles with diameters ranging from 0.25 to 4 mm, sourced from the Yangtze River. These particle patterns were magnified 5-10 times to generate two-dimensional images. Subsequently, the software's built-in algorithms were used to integrate morphological data across various scales, thereby delineating the contours of the fine particle targets. Each particle was then identified and localized to facilitate the extraction, analysis, and calculation of shape parameters associated with their two-dimensional images.

2.3.2 Particle geometric features

2.3.2.1 Sphericity coefficient

The sphericity coefficient is a dimensionless parameter used to quantify the degree to which a particle resembles a spherical shape. For a given sediment particle, the sphericity coefficient can be calculated using the principle of spherical harmonics, as illustrated in Equation 1. However, due to the challenges associated with directly measuring the particle's volume and determining the equivalent radius, an approximate method is utilized. This approach estimates the equivalent radius based on the ratio of the particle's axes. In practice, the long, middle, and short axes of sediment particles from the YRSA were measured using vernier calipers. The sphericity coefficient, denoted as SI, was subsequently calculated using Equation 2.

The sediment particles were divided into seven grain size groups: 0.5-1 mm, 1-2 mm, 2-4 mm, 4-8 mm, 8-16 mm, 16-32 mm, and >32 mm. For each group, 50 particles were randomly selected and tested, and the average value was determined.

$$SI = \frac{4\pi}{S}\left(\frac{3V}{4\pi}\right)^{\frac{2}{3}} \tag{1}$$

$$SI = \sqrt[3]{\left(\frac{M}{L}\right)^{2}\left(\frac{S}{M}\right)} \tag{2}$$

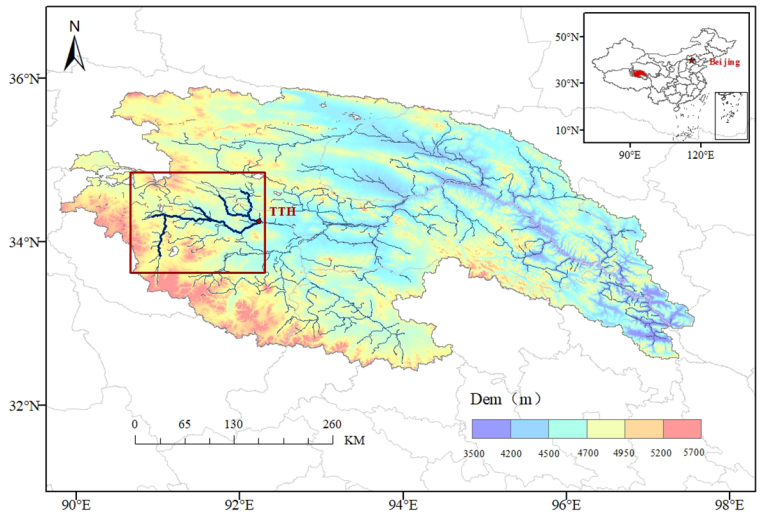

FIGURE 1
Regional overview of the Yangtze River source area.

FIGURE 2
Sediment sampling location **(A)** river islands **(B)** point bars **(C)** riverbed.

in which S represents the area of the sediment particle (unit: m^2), V represents the volume of the sediment particle (unit: m^3), and L, M, and S denote the lengths of the long, middle, and short axes of the sediment particles, respectively (unit: m).

2.3.2.2 Triaxial shape coefficient

The triaxial shape coefficient is used to describe the shape characteristics of particles in three-dimensional space. It quantifies the relative size differences of particles along their three principal dimensions: the long axis, the middle axis, and the short axis. This metric helps to reflect the regularity or irregularity of the particle shape. Specifically, the shape changes of particles in these three dimensions are estimated by integrating the ratios of the axis lengths. The calculation is provided by Equation 3:

$$SF = \frac{S}{\sqrt{LM}} \tag{3}$$

in which SF represents the triaxial shape coefficient, while L, M, and S denote the lengths of the long, middle, and short axes of the sediment particles, respectively (unit: m).

2.3.3 Particle density measurement

The specific gravity of sediment particles is the ratio of the mass of sediment dried to a constant weight at 105-110°C to the mass of pure water at 4°C of the same volume. Numerically, it is the same as the relative density of soil particles and is a dimensionless quantity that is an important indicator for measuring the compactness of soil particles.

The specific gravity bottle method was adopted in the experiment to measure the specific gravity of soil particles G_S, in accordance with the "Standard for Geotechnical Test Methods (GBT 50123-2019)". 15 grams of soil samples dried to a constant weight were placed in a calibrated 100 ml specific gravity bottle, an appropriate amount of pure water was injected and boiled for 1.5 hours to completely eliminate the air in the soil. After cooling, the bottle was filled with pure water again and placed in a constant temperature water bath. When the suspension clarified, the total mass of the bottle, water, and soil, as well as the water temperature, were recorded. The data were corrected based on the pre-drawn curve of bottle water mass and temperature. Parallel experiments were conducted simultaneously, and the arithmetic average was taken to ensure that the error of the two measurements was less than 0.02 grams. The calculation Equation is as follows:

$$G_S = \frac{m_s \cdot \rho_{\omega t}}{(m_s + m_{bw} - m_{bws})} \tag{4}$$

In which m_s represents the dry soil mass (unit: g), $\rho_{\omega t}$ is liquid density (unit: g/cm^3), m_{bw} is the total mass of the specific gravity bottle and liquid (unit: g), m_{bws} is the total mass including the specific gravity bottle, liquid, and soil (unit: g); $m_s + m_{bw} - m_{bws}$ is the mass equivalent to the dry soil volume immersed in liquid (unit: g).

2.3.4 Sediment gradation

Sediment gradation, which relies on detailed particle size distribution data, directly reflects the characteristics of the parent rock, the degree of water flow sorting, and the transport characteristics. It indicates the coarseness and distribution balance of sediment particles and is a key indicator for measuring the particle size distribution in sand samples. Compared to traditional sieve analysis, the laser particle size analyzer (LPSA) is unaffected by particle shape and density, thus providing a more accurate representation of the size characteristics of sediment particles. A recent study compared LPSA with other laboratory techniques, such as optical point counting, 2D automated image analysis, and X-ray computed tomography. The LPSA integrates advanced laser diffraction technology with Mie scattering theory and is capable of delivering high-precision and high-resolution particle size distribution data (50, 51).

In this study, the Mastersizer 3000 laser particle size analyzer was employed to determine the particle size distribution of the samples. The sediment samples were uniformly dispersed in water and then introduced into the sample cell using the Hydro MV wet dispersion unit, with the stirring speed set at 2500 rpm, ultrasonic power at 40W, and ultrasonic time at 1 minute. During the measurement, the instrument measured the intensity of the scattered light via laser diffraction technology and calculated the

10.3389/fsoil.2025.1540941

FIGURE 3
Laser particle size analyzer (Mastersizer 3000E).

particle size distribution based on Mie's theory. After the measurement, the data were analyzed and processed using the instrument's software to generate particle size distribution charts and related statistical data. The equipment is shown in Figure 3.

2.3.5 Particle accumulation state

Particle irregularity significantly influences the accumulation state. The angle of repose characterizes the critical slope stability angles of sediment particle accumulation and serves as an indispensable quantitative index in complex accumulation phenomena.

In this experiment, the sliding plate method was employed to measure the angle of repose for sediment. Compared to the disc and funnel methods, it effectively overcomes measurement errors caused by "top cutting" and "arc transition" effects, making it applicable to a wider range of particle sizes and simpler to operate underwater. The sediment samples collected from the Tuotuo River riverbed were classified into five grain size groups using the sieve analysis method: less than 5 mm, 5-10 mm, 10-12 mm, 12-15 mm, and greater than 15 mm. These groups are designated Groups I to V, respectively, while the non-uniform original sand samples are called Group VI. The instrument consists of a rectangular tank (50 cm in length, 20 cm in width, 35 cm in height), which is evenly divided into two areas by a movable baffle (20 cm in width, 40 cm in height), as shown in Figure 4. During the measurement process, the baffle is smoothly withdrawn, allowing the sediment particles to slide under gravity and form a natural slope. Repeated measurements are taken using the following Equation:

$$\varphi = \arctan\left(\frac{h}{a}\right) \tag{5}$$

in which φ represents the angle of repose (unit: °), a is the base length of the natural slope (unit: m), and h is the extended height of the accumulated body (unit: m).

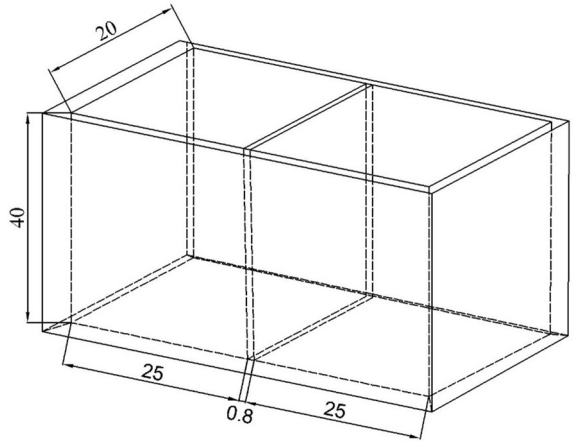

FIGURE 4
Schematic diagram of the plexiglass sink (unit: cm).

2.3.6 Chemical composition of sediment

In this experiment, a SmartLab SE X-ray diffractometer was utilized to conduct phase analysis of the sediment samples. A 0.5-gram sample of finely ground and sieved powder (200-mesh) was placed in the grooves of a glass carrier. A clean ground glass sheet was used to compact and flatten the sample, ensuring that the surface was level with the edge of the groove. The sample was then placed in the diffractometer for testing. The test employed a copper target as the X-ray source, with a tube voltage of 40 kV, a current of 40 mA, a scanning speed of 2°/min, a step size of 0.02°, and a range of 5-90°.

A Rigaku ZSX Primus III+ X-ray fluorescence spectrometer was used to analyze the elemental and oxide content of the sediment samples. The samples were prepared into uniform pressed tablets with a diameter of 20 mm using a hydraulic press and then placed in the sample box. The test conditions were set to use an Rh target X-ray tube with a maximum power of 3 kW, ensuring wide element coverage from sodium (Na, Z = 11) to uranium (U, Z = 92). High-sensitivity and high-resolution analysis of the sample composition were achieved through the combined use of scintillation counters (SC) and proportional counters (PC), along with precise 2θ scanning goniometer technology.

3 Results

3.1 Particle morphological characteristics

Using the analysis software, sediment particle patterns with diameters ranging from 0.25 to 4 mm, sourced from the Yangtze River, were magnified 5 to 10 times to allow for an intuitive observation of their morphology, as depicted in Figure 5. This figure shows the grain shapes of sediment samples with varying grain sizes. Some particles exhibited shapes that were nearly circular or elliptical, while others displayed irregular polygonal or angular forms. As particle size increased, the morphology became more irregular. This irregularity is attributed to the short transport distance of the sediment and the limited number of collisions among sediment particles in the source area, resulting in more pronounced angularity.

3.2 Particle geometric characteristics

As shown in Table 1, which presents the geometrical characteristics of sediment particles, the sphericity coefficient ranges from 0.650 to 0.737, with an average of 0.685. This is significantly lower than the average sphericity coefficient of 0.86 for natural sand in non-plateau regions (52). The triaxial shape coefficient varies from 0.471 to 0.661, with an average of 0.541, which is notably smaller than the average of 0.78 for sediment in the natural state in non-plateau areas.

Analysis indicates that sediment particles in the Yangtze River source region exhibit a more pronounced non-spherical tendency. In three-dimensional form, they are flatter and more elongated, rather than tending towards an isotropic shape. This morphological disparity reflects the long-term influence of different sedimentary environments. In the plateau region, characterized by high altitude, steep slopes, and rapid water flow, sediment particles undergo intense scouring and collisions during transportation, resulting in their distinctive morphological characteristics.

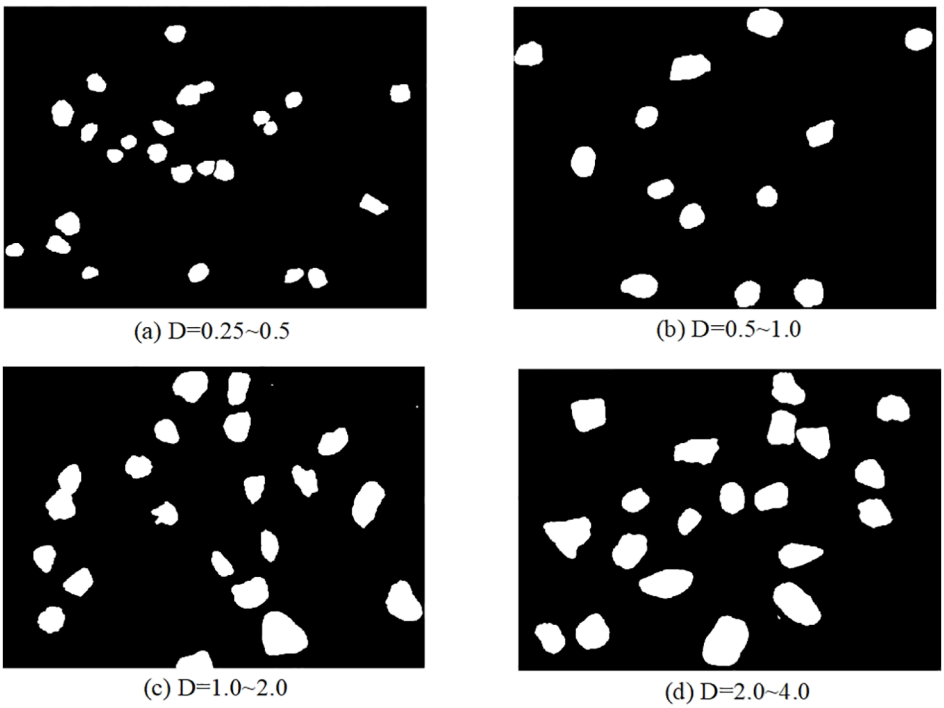

FIGURE 5
Grain shape of sediment samples with different grain sizes (unit: mm): **(A)** D=0.25~0.5; **(B)** D=0.5~1.0; **(C)** D=1.0~2.0; **(D)** D=2.0~4.0.

10.3389/fsoil.2025.1540941

TABLE 1 Geometrical characteristics of sediment particles.

Sediment particle size (mm)	Spherical coefficient	Three axis shape coefficient
>32	0.650	0.471
16-32	0.691	0.488
8-16	0.687	0.529
4-8	0.663	0.478
2-4	0.737	0.661
1-2	0.695	0.639
0.5-1	0.671	0.522
/	0.685	0.541

TABLE 2 Specific gravity of sediment particles.

Sediment particle size (mm)	Specific gravity
2-4	2.692
1-2	2.689
0.5-1	2.691
0.125-0.5	2.695
<0.125	2.654

3.3 Particle density

The density of non-uniform sediment particles is 2.77×10^3 kg/m^3, and the dry density is 1.917×10^3 kg/m^3. For uniform sediment particles, the density distribution of particles smaller than 4 mm is presented in Table 2. The specific gravity of sediment particles averages 2.70×10^3 kg/m^3. In the Yangtze River source region, sediment particles exhibit porosity when accumulated as dry sand, indicating that the compactness between sediment particles is relatively low, with more voids present.

3.4 Sediment gradation

The soil engineering classification adheres to the current standards of geotechnical test methods (GBT 50123-2019). Based on the grain size distribution in 2023, the sediments in the Tuotuo River are primarily composed of fine-grained and coarse-grained soils. The sediment grain size composition is predominantly coarse sand (0.5-2.0 mm), fine gravel (2.0-5.0 mm), and medium gravel (5.0-20.0 mm), which together account for approximately 72% of the total. The other grain size components and their proportions are as follows: clay particles (<0.005 mm) make up 3%, silt particles (0.005-0.075 mm) constitute 5%, fine sand (0.075-0.25 mm) is 9.5%, medium sand (0.25-0.50 mm) is 9.5%, and coarse gravel (20-60 mm) is 1%. The gradation of sediment samples is shown in Figure 6.

By comparing the sediment grain size changes from 2016 to 2023, it has been observed that the composition of riverbed sediment at the source of the Yangtze River has undergone significant alterations in recent years. The D10 value has increased from 0.0026 mm to 0.15 mm, and the D50 value has risen from 0.12 mm to 1.8 mm. The cumulative proportion of sediment with a particle size smaller than 0.1 mm has decreased significantly by 37.2%, while the cumulative proportion of sediment with a particle size larger than 1 mm has increased substantially by 60.3%, indicating a stable growth trend.

Grain size characteristics reflect the sources of sediments and the conditions of depositional dynamics. Sediment grain size is related to the composition of the parent rock and is directly associated with the depositional environment, thereby directly reflecting the content and distribution of sediment composition. The sediments of the Yellow River Delta, transported over long distances, are primarily composed of silt (58%) and sand (77.9%) (43), with the depositional environment influenced by both fluvial and marine dynamics. In contrast, sediments from YRSA are predominantly coarse sand and gravel (72%), exhibiting greater resistance to weathering. These sediments have a short transport distance and originate mainly from rock debris and soil particles produced by intense weathering processes.

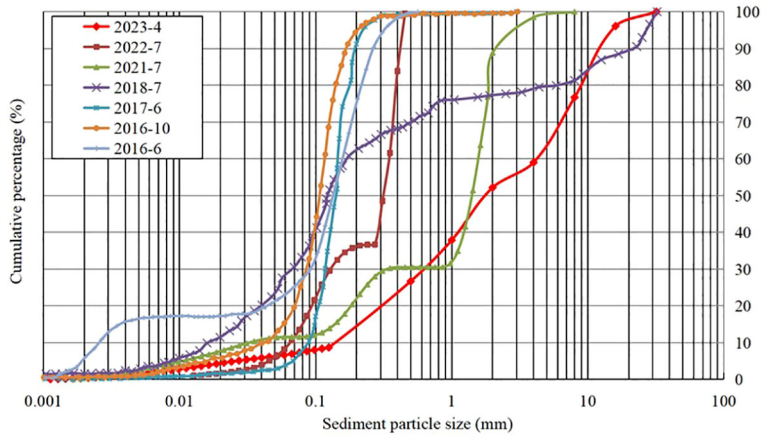

FIGURE 6
Gradation of sediment samples with different grain sizes.

3.5 Particle pileup state

Sediment samples from groups I to VI were collected and tested using the draw-plate method in a rectangular glass tank. The experiment was divided into two parts to measure the angle of repose for each sample group, both in air and submerged in water. After filling the tank with sand (and water), the baffle was gradually removed, allowing the samples to slide under gravity and eventually form a stable slope. The slope gradient represents the angle of repose on the water surface (or underwater). This angle significantly reflects the interactions between sediment particles and the medium (water), as well as the mechanical stability among the particles. The test process is illustrated in Figure 7.

In the angle of repose test, the angles on the front and back of the slope were calculated separately, and the average was taken as the test result for that instance. To accurately simulate the state of sediment in still water, when measuring the underwater angle of repose, clear water was poured into the left area (vacant state) and slowly flowed into the right area (with test materials) due to the small gap between the baffle and the tank bottom. Measurements were conducted after the clear water completely submerged the sediment particles, and the water surface in the two areas separated by the baffle became stable. The results obtained by repeating the test and averaging the values are presented in Table 3.

The above-water angle of repose (36.7°) and underwater angle of repose (35.9°) of non-uniform sediment in the Yangtze River source region are both higher than the typical range for irregular natural sediment in non-source regions (31.4° to 34.8°) (53, 54). For engineering projects or research related to riprap revetment, local scour around bridge piers, sand selection for river engineering models, and the initiation and transport rate of bed load sediment in the Yangtze River source region, the differences from non-source regions must be considered, and conventional theories or engineering practices cannot be simply applied.

Similarly, consistent with other studies (53, 55, 56), the above-water angle of repose of uniform sediment in the Yangtze River source region (35.5° to 38.7°) is higher than the underwater angle of repose (34.9° to 36.8°), and this disparity increases with larger particle sizes, as shown in Figure 8. This suggests that the angle of repose is influenced not only by the particle size of the sediment but also by its gradation and shape.

3.6 Chemical composition of sediment

The MDL Jade 9.0 software was used to analyze the mineral composition of sediment particles smaller than 0.075 mm in the Yangtze River source region, based on XRD spectrum data. The primary mineral search results are depicted in Figure 9. The irregular sediment in this region is predominantly composed of anorthite, quartz, calcite, and mica, with heavy minerals constituting 13.3% of the total composition (as shown in Table 4). In contrast, in the sediment deposits at the Yangtze River estuary, the heavy mineral content of sediment with a particle size of 0.01-0.1 mm is approximately 5% (57). This

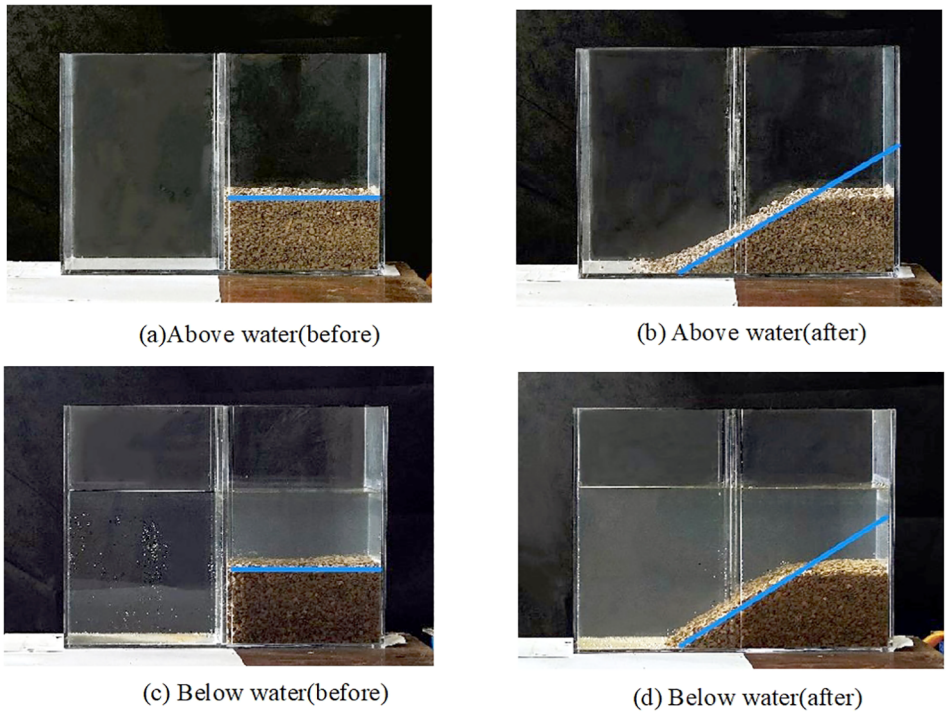

FIGURE 7
Measurement of angle of repose above water and below water: **(A)** Above water (before); **(B)** Above water (after); **(C)** Below water (before); **(D)** Below water (after).

10.3389/fsoil.2025.1540941

TABLE 3 Angle of repose above water and below water (unit: °).

Sediment particle size (mm)	Above water	Below water
<5	35.5	34.9
5-10	36.1	35.1
10-12	37.5	36.2
12-15	37.6	37.0
>15	38.8	36.6
All	36.7	35.9

significant decrease in heavy mineral content from upstream to downstream indicates that the predominant sedimentary layers along the river course from the source region to the estuary are composed of lighter minerals.

Quantitative analysis was conducted using the K-value method, and the mineral composition is detailed in Table 4. The main components include SiO_2, $CaCO_3$, (Ca, Na)(Si, Al)$_4O_8$, and (K, Na)(Al, Mg, Fe)$_2$(Si$_{3.1}$Al$_{0.9}$)O$_{10}$(OH)$_2$, with SiO_2 being the most abundant. The relative stability of the minerals was also analyzed, revealing that stable minerals such as quartz and feldspar account for 75.2%, while the remaining minerals are primarily mica and chlorite. The chemical composition of sediment in the Yangtze River source region is predominantly SiO_2, CaO, and Al_2O_3, aligning with the sediment's mineral composition, which is mainly quartz, feldspar, calcite, and mica. Other components include Fe_2O_3, K_2O, MgO, and Na_2O, which are associated with heavy minerals containing iron and manganese, such as magnetite and limonite. The contents of TiO_2, P_2O_5, MnO, and BaO are relatively low. As indicated in Table 5, the elemental analysis of sediment particles in the Yangtze River source region shows that O, Si, and Ca are the major elements. The main trace elements are Ti,

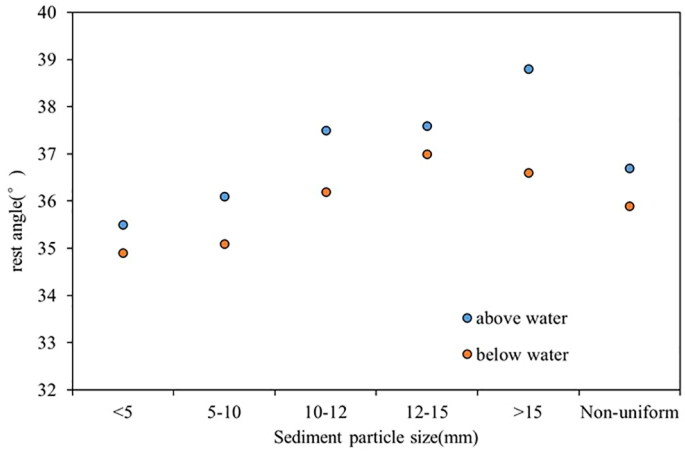

FIGURE 8
Resting angle of sediment in the Yangtze River source area.

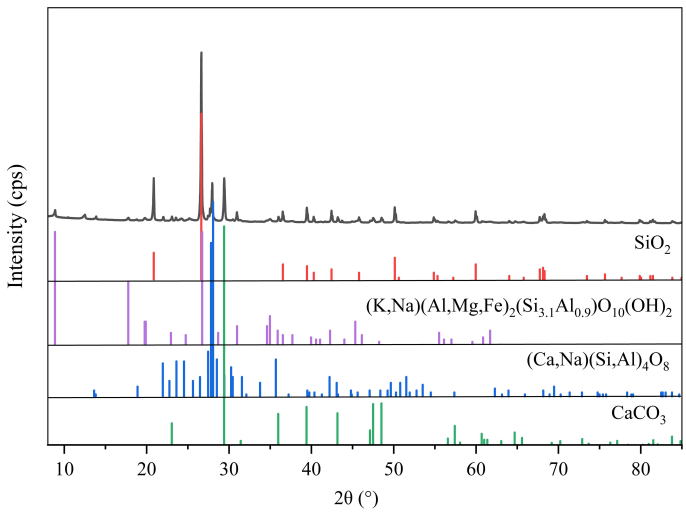

FIGURE 9
XRD patterns of sediment samples (major compounds).

10.3389/fsoil.2025.1540941

TABLE 4 Mineral compositions of samples (%).

Chemical components	Chemical formula	wt.%
Quartz	SiO_2	33.7
Albite	$Na_{0.98}Ca_{0.02}Al_{1.02}Si_{2.98}O_8$	6.3
Calcite	$CaCO_3$	6.3
Muscovite	(K, Na)(Al, Mg, Fe) $_2(Si_{3.1}Al_{0.9})O_{10}(OH)_2$	9.4
Clinochlore	$Al_2Mg_5(Si_3O_{10})(OH)_8$	2.1
Dolomite	$CaMg(CO_3)_2$	1.8
Cristobalite	SiO_2	1.2
Anorthite	$(Ca, Na)(Si, Al)_4O_8$	34.0

Mn, Ba, P, Sr, Zr, and Cl, while the concentrations of Ni, Cu, As, Co, and other elements are extremely low. Among the heavy metal elements, including Zn, Ba, Sr, Zr, Rb, Ni, Cu, As, Co, and Y, they collectively represent 0.14% of the composition.

TABLE 5 Percentage of oxides and elements in sediment (%).

Oxides	(%)	Elements	(%)
SiO_2	52.3363	O	50.6958
CaO	19.6094	Si	22.0593
Al_2O_3	13.9708	Ca	12.0017
Fe_2O_3	6.2457	Al	6.7904
K_2O	2.7013	Fe	3.6138
MgO	2.0359	K	1.9451
Na_2O	1.0468	Mg	1.1373
TiO_2	0.8635	Na	0.7246
SO_3	0.4544	Ti	0.4320
P_2O_5	0.1814	S	0.1590
MnO	0.1426	Mn	0.0915
BaO	0.1171	Ba	0.0867
SrO	0.0872	P	0.0693
ZrO_2	0.0828	Sr	0.0600
ZnO	0.0265	Zr	0.0499
V_2O_5	0.0257	Cl	0.0201
Cl	0.0230	Zn	0.0174
Rb_2O	0.0163	V	0.0123
NiO	0.0101	Rb	0.0121
CuO	0.0073	Ni	0.0065
As_2O_3	0.0068	Cu	0.0047
Co_2O_3	0.0055	As	0.0042
Y_2O_3	0.0036	Co	0.0036

The elemental composition of sediments is influenced by particle size and depositional environment. Fine-grained sediments, such as clay and silt, typically contain higher hydrophilic minerals, including clay and fine-grained carbonate minerals. The sediments of the Yellow River Delta, located near the river mouth and influenced by marine conditions, have transitioned from fluvial deposition to nearshore wave erosion. These sediments exhibit elevated concentrations of trace elements such as Cl, Mn, and Ba (58). In contrast, sediments from YRSA have not experienced extensive mineralogical sorting and are primarily composed of feldspar and quartz, which exhibit low chemical reactivity. Consequently, the elemental composition of YRSA sediments is relatively stable, mainly comprising elements like silicon (Si), calcium (Ca), aluminum (Al), and iron (Fe).

4 Conclusion and future perspectives

1. The sphericity coefficient of sediment particles in the Yangtze River source region is 0.69, and the triaxial shape coefficient is 0.554, both indicating relatively low values. This suggests that the particles are more irregular and angular compared to those in non-plateau regions, exhibiting a pronounced non-spherical tendency and a flatter, elongated form in three dimensions.
2. The density of sediment particles is 2.77×10^3 kg/m^3, while the dry density is 1.917×10^3 kg/m^3, indicating the presence of numerous voids. The particle size composition primarily consists of coarse sand, fine gravel, and medium gravel, showing a coarsening trend. The water surface angle of repose for irregular sediment in the Yangtze River source region is 36.7°, and the underwater angle of repose is 35.9°. The angle of repose for uniform sediment is generally higher than in non-plateau regions, resulting in poorer fluidity.
3. The sediment in the Yangtze River source region is predominantly composed of minerals such as quartz and feldspar. Minerals with a hardness of ≥ 7 account for approximately 70%, and the sediment is angular and highly resistant to chemical weathering. The chemical composition is dominated by SiO_2, CaO, and Al_2O_3, with trace elements such as Ti, Mn, Ba, P, Sr, Zr, and Cl being the most abundant.

This study highlights the unique characteristics of sediments in the YRSA, which include a higher proportion of hard minerals such as quartz and feldspar, angular grain morphology, low mobility, and high resistance to chemical weathering. These features set them apart from sediments in non-headwater areas. Consequently, when undertaking riverbank slope-related projects or research in the Yangtze headwater region, it is crucial to consider these distinct attributes and refrain from applying conventional theories or engineering practices indiscriminately.

The research findings offer valuable insights for designing water conservancy projects in the Yangtze headwater region, especially in selecting bank protection materials and predicting sedimentation

and erosion processes. The hard minerals prevalent in this area, characterized by their high strength and chemical stability, make them ideal for bank protection. Moreover, the angularity and low mobility of sediment particles can enhance riverbank stability when suitable bank protection structures and layouts are employed. By integrating the physical properties of sediments with flow conditions and riverbed morphology, we can more accurately forecast the future evolution of rivers. This, in turn, provides a robust scientific foundation for engineering design, ensuring effective flood control, irrigation, and power generation projects in the Yangtze headwater region.

Looking ahead, future research could focus on the temporal and spatial variations in sediment characteristics, as well as the initiation characteristics of sediment in the Yangtze headwater region, aiming to deepen our understanding of sediment transport mechanisms within the dynamic context of glaciers and permafrost in the source area. Additionally, the study can explore the impacts of climate change on sediment erosion, transport, and deposition, with a particular focus on the potential effects of glacier melting and permafrost degradation. These investigations will be vital in supporting environmental impact assessments, developing adaptive climate policies, addressing climate change and its associated risks, and achieving sustainable regional development in the Yangtze headwater region.

Data availability statement

The original contributions presented in the study are included in the article/supplementary material. Further inquiries can be directed to the corresponding authors.

Author contributions

ZL: Conceptualization, Formal analysis, Methodology, Writing – review & editing. XW: Conceptualization, Formal analysis, Methodology, Writing – original draft. YL: Conceptualization, Methodology, Validation, Writing – review & editing. WL: Formal analysis, Software, Supervision, Writing – review & editing. XZ: Funding acquisition, Investigation, Project administration, Writing – review & editing. CL: Funding acquisition, Investigation, Project administration, Writing – review & editing. GW: Formal analysis, Methodology, Software, Writing – review & editing. JM: Data curation, Investigation, Resources, Writing – review & editing.

Funding

The author(s) declare financial support was received for the research, authorship, and/or publication of this article. The authors declare that this study received funding from the National Natural Science Foundation of China (52239007, U2240226, 52479058), the National Key Research and Development of China (2022YFC3201703-05, 2023YFC3209505), the National Young Top-notch Talent Support Program, the Central Public-interest Scientific Institution Basal Research Fund (CKSF20241011/HL, CKSG2024985/HL, CKSF2024324/HL), the Open Fund Research of State Key Laboratory of Hydraulics and Mountain River Engineering (Sichuan University) (SKHL2311), and the Research Project of China Three Gorges Corporation (0704230). The funder was not involved in the study design, collection, analysis, interpretation of data, the writing of this article, or the decision to submit it for publication.

Conflict of interest

Author CL was employed by China Three Gorges Corporation.

The remaining authors declare that the research was conducted in the absence of any commercial or financial relationships that could be construed as a potential conflict of interest.

Generative AI statement

The author(s) declare that no Generative AI was used in the creation of this manuscript.

Publisher's note

References

1. Li Z, Guo X, Yang Y, Hong Y, Wang Z, You L. Heatwave Trends and the Population Exposure over China in the 21st Century as Well as under 1.5°C and 2.0°C Global Warmer Future Scenarios. *Sustainability*. (2019) 11:3318. doi: 10.3390/su11123318

2. López-Moreno JI, Pomeroy JW, Morán-Tejeda E, Revuelto J, Navarro-Serrano FM, Vidaller I, et al. Changes in the frequency of global high mountain rain-on-snow events due to climate warming. *Environ Res Lett*. (2021) 16(9):094021. doi: 10.1088/1748-9326/ac0dde

3. Calvin K, Dasgupta D, Krinner G, Mukherji A, Thorne PW, Trisos CH, et al. *Ipcc, 2023: climate change 2023: synthesis report*. Geneva, Switzerland: Synthesis Report (2023).

4. Ma J, Ren HL, Mao X, Liu M, Wang T, Ma X. Spatiotemporal Evolution Disparities of Vegetation Trends over the Tibetan Plateau under Climate Change. *Remote Sens*. (2024) 16:2585–. doi: 10.3390/RS16142585

5. Zhang H, Mu X, Meng F, Zheng E, Dong F, Li T, et al. Future increase in extreme precipitation: historical data analysis and influential factors. *Sustainability*. (2024) 16:9887. doi: 10.3390/su16229887

6. Du J, Yu X, Zhou L, Li X, Ao T. Less concentrated precipitation and more extreme events over the three river headwaters region of the tibetan plateau in a warming climate. *Atmospheric Res*. (2024) 303:107311. doi: 10.1016/J.ATMOSRES.2024.107311

7. Wang L, Zhao L, Zhou H, Liu S, Liu G, Zou D, et al. Quantification of water released by thawing permafrost in the source region of the yangtze river on the tibetan plateau by insar monitoring. *Water Resour Res*. (2023) 59. doi: 10.1029/2023WR034451

8. Tianyu F, Zhiliang M, Yuan D. *The changjiang river civilization*. Singapore: Springer Nature Singapore (2023).

9. Zhang Y, Liu S, Xu J, Shangguan D. Glacier change and glacier runoff variation in the tuotuo river basin, the source region of yangtze river in western China. *Environ Geology*. (2007) 56:59–68. doi: 10.1007/s00254-007-1139-2

10. Hu G, Dong Z, Lu J, Yan C. Driving forces responsible for aeolian desertification in the source region of the yangtze river from 1975 to 2005. *Environ Earth Sci*. (2012) 66:257–63. doi: 10.1007/s12665-011-1235-1

11. You Q, Cai Z, Pepin N, Chen D, Ahrens B, Jiang Z, et al. Warming amplification over the arctic pole and third pole: trends, mechanisms and consequences. *Earth-Science Rev*. (2021) 217:103625. doi: 10.1016/j.earscirev.2021.103625

12. Ding Y, Zhang S, Zhao L, Li Z, Kang S. Global warming weakening the inherent stability of glaciers and permafrost. *Sci Bull*. (2018) 64:245–53. doi: 10.1016/j.scib.2018.12.028

13. Huang T, Shen P. Stability of moraine deposits under changing climate on the tibetan plateau. In: *Geo-risk 2023*. American Society of Civil Engineers, Arlington, Virginia (2023). p. 127–36.

14. Ma X, Wang X, Gao Y, Yue F, Chen W. Geochemical indicators on the central tibetan plateau lake sediments: historical climate change and regional sustainability. *Sustainability*. (2024) 16:8186–. doi: 10.3390/su16188186

15. Taigang Z, Weicai W, Ziheng S, Baosheng A. Increasing frequency and destructiveness of glacier-related slope failures under global warming. *Sci Bull*. (2023) 69:30–3. doi: 10.1016/J.SCIB.2023.09.042

16. Li Y, Wang Y, Wang X, Qi J, Zhang X, Lin Q. Risk assessment of glacial debris flow on highway under warming climate: A case study of tianmo gully in the southeastern tibetan plateau. *Ecol Indic*. (2024) 167:112606–. doi: 10.1016/J.ECOLIND.2024.112606

17. Liu Y, Qiu H, Wang J, Wang N, Jiang X, Tang B, et al. Prominent creep characteristics of thermokarst landslides on central tibetan plateau under climate warming conditions. *Catena*. (2024) 246:108457–. doi: 10.1016/J.CATENA.2024.108457

18. Kaisheng L. Contribution of ecological conservation programs and climate change to hydrological regime change in the source region of the yangtze river in China. *Regional Environ Change*. (2022) 22. doi: 10.1007/S10113-021-01874-Z

19. Luo K. Contribution of ecological conservation programs and climate change to hydrological regime change in the source region of the Yangtze river in China. *Reg. Environ. Change*. (2022) 22(1):1–24. doi: 10.1007/s10113-021-01874-z

20. Shi C, Zhang DD, You L. Sediment budget of the yellow river delta, China: the importance of dry bulk density and implications to understanding of sediment dispersal. *Mar Geology*. (2003) 199:13–25. doi: 10.1016/S0025-3227(03)00159-2

21. Zhao C, Fang H, Liu Y, Dey S, He G. Impact of particle shape on saltating mode of bedload transport sheared by turbulent flow. *J Hydraulic Eng*. (2020) 146:04020034–. doi: 10.1061/(ASCE)HY.1943-7900.0001735

22. Jing Y, Zhang J, Zhang Q, Maa JPY. Experimental study on the effects of sediment size gradation and suspended sediment concentration on the settling velocity, ws. *Powder Technol*. (2024) 437:119541–. doi: 10.1016/J.POWTEC.2024.119541

23. Li P, Hu K, Yu J. Experimental investigation on the permeability and fine particle migration of debris-flow deposits with discontinuous gradation: implications for the sustainable development of debris-flow fans in jiangjia ravine, China. *Sustainability*. (2024) 16:10066–. doi: 10.3390/SU162210066

24. Tian W, Peng L, Jingming H, Yu T, Jing L, Feng W, et al. Transport mechanism of eroded sediment particles under freeze-thaw and runoff conditions. *J Arid Land*. (2022) 14:490–501. doi: 10.1007/S40333-022-0016-X

25. Wang S, Fan Y, Liu L, Qu J. Transport/detachment regimes of different size class sediment particles and enlightenments for transport capacity prediction for rain-induced overland flow erosion. *Sustainability*. (2023) 15(10):7906. doi: 10.3390/SU15107906

26. Jiao J, Wang Z, Zhao G, Wang W, Mu X. Changes in sediment discharge in a sediment-rich region of the yellow river from 1955 to 2010: implications for further soil erosion control. *J Arid Land*. (2014) 6:540–9. doi: 10.1007/s40333-014-0006-8

27. Hu D, Li S, Jin Z, Lu S, Zhong D. Sediment transport and riverbed evolution of sinking streams in a dammed karst river. *J Hydrology*. (2020) 596:125714. doi: 10.1016/j.jhydrol.2020.125714

28. Martellotta AMN, Levacher D, Gentile F, Piccinni AF. Estimation of silting evolution in the camastra reservoir and proposals for sediment recovery. *J Mar Sci Eng*. (2024) 12. doi: 10.3390/JMSE12020250

29. Zilin S, Hua W, Dongfang L, Yiping L, Wenbo S, Yuanyuan L. Physicochemical properties of suspended sediment in typical waters of the mid-lower yangtze river basin. *Hydrological Sci J*. (2022) 67:1892–903. doi: 10.1080/02626667.2022.2099282

30. Nana W, Jian L, Zicheng Z, Tingxuan L, Shuqin H, Yonghua Z, et al. Upslope inflow-driven variations in microtopography and size fractions effect on rill erosion in purple soil hillslopes. *J Hydrology*. (2023) 622:129759. doi: 10.1016/J.JHYDROL.2023.129759

31. Bulteau T, Marteau B, Batalla RJ, Chapron E, Valette P, Piégay H. Effects of repeated drawdown flushing on riverbed fine sediment dynamics downstream from a dam. *Anthropocene*. (2024) 47:100444–. doi: 10.1016/j.ancene.2024.100444

32. Beaumont H, Ockelford A, Simpson PM. Sand bed river dynamics controlling microplastic flux. *Sci Rep*. (2024) 14:29420. doi: 10.1038/S41598-024-80892-3

33. Chen W, Xu J, Wang S, Chen Z, Dong S. Key drivers of heavy metal bioavailability in river sediments and microbial community responses under long-term high-concentration pollution. *Environ Res*. (2025) 265:120375. doi: 10.1016/j.envres.2024.120375

34. Turley MD, Bilotta GS, Arbociute G, Chadd RP, Extence CA, Brazier RE. Quantifying submerged deposited fine sediments in rivers and streams using digital image analysis. *River Res Appl*. (2017) 33:1585–95. doi: 10.1002/rra.3073

35. Wang H, Shen Z, Yan Y, Liang D. Assessment of physicochemical properties of suspended sediment in yangtze river estuary. *Phys Geogr*. (2024) 45:39–52. doi: 10.1080/02723646.2023.2217059

36. Zhang N, Fu K, Han Y, Huang Y, Xin P. Spatial and temporal variability of physicochemical characteristics in lancang river sediments amid hydropower development. *Sci total Environ*. (2024) 958:177737. doi: 10.1016/J.SCITOTENV.2024.177737

37. Guerrero Fernández E, Díaz M, Wei Y, Moore C. Modeling sediment movement in the shallow-water framework: A morpho-hydrodynamic approach with numerical simulations and experimental validation. *Ocean Model*. (2024) 192:102445–. doi: 10.1016/j.ocemod.2024.102445

38. Xie R, Lin P. Numerical modeling of sediment dumping in deep water through a rock-fall pipe for subsea pipeline burial. *Appl Ocean Res*. (2025) 154:104328–. doi: 10.1016/J.APOR.2024.104328

39. Visher GS. Grain size distributions and depositional processes. *J Sedimentary Res*. (1969) 39:1074–106.

40. Moayeri Kashani M, Hin L, Ibrahim S, Nik Sulaiman N, Teo F. An investigation into the effects of particle texture, water content and parallel plates' Diameters on rheological behavior of fine sediment. *Int J Sediment Res*. (2016) 31:120–30. doi: 10.1016/j.ijsrc.2015.11.001

41. Li S, Zhu M, Huang W, Zhu H, Zhang R, Lu Y. On Sediment incipient motion of marine cohesive sediments with different bulk densities. *Geomorphology*. (2023) 441:108918-. doi: 10.1016/j.geomorph.2023.108918

42. Cassel M, Lave J, Recking A, Malavoi JR, Piegay H. Bedload transport in rivers, size matters but so does shape. *Sci Rep*. (2021) 11:508. doi: 10.1038/s41598-020-79930-7

43. Meng L, Wang L, Zhao J, Zhan C, Liu X, Cui B, et al. End-member characteristics of sediment grain size in modern yellow river delta sediments and its environmental significance&13. *Front Mar Sci*. (2023) 10. doi: 10.3389/FMARS.2023.1141187

44. Li J, Wang G, Sun S, Ma J, Guo L, Song C, et al. Mapping and reconstruct suspended sediment dynamics (1986–2021) in the source region of the yangtze river, qinghai-tibet plateau using google earth engine. *Remote Sens Environ*. (2025) 317:114533. doi: 10.1016/j.rse.2024.114533

45. Mingxiao L, Yongjie Z, Zixi Z, Dongpo S. Bimodal bed load transport characteristics under the influence of mixture ratio. *Water*. (2023) 15:487. doi: 10.3390/w15030487

46. Shayan N, Hojat K, Khosrow H. Effect of sediment gradation on scour by symmetric crossing jets: an experimental investigation. *Water Supply*. (2022) 22:8211–32. doi: 10.2166/WS.2022.349

47. Wang Y, Li H, Mou C, Chen W, Gao C, Liang W, et al. Sedimentary characteristics and evolution of the upper permian wujiaping formation in the eastern yangtze block. *Front Earth Sci*. (2024) 12:1450872–. doi: 10.3389/feart.2024.1450872

48. He Z, Li F, Dominech S, Wen X, Yang S. Heavy metals of surface sediments in the changjiang (Yangtze river) estuary: distribution, speciation and environmental risks. *J Geochemical Explor*. (2018) 198:18–28. doi: 10.1016/j.gexplo.2018.12.015

49. Zhiwei L, Hanyou L, Peng G, Yuchi Y, Xuyue H. Characterizing braided rivers in two nested watersheds in the source region of the yangtze river on the qinghai-tibet plateau. *Geomorphology*. (2019) 351:106945. doi: 10.1016/j.geomorph.2019.106945

50. Elisabeth S, Mikaela M. Grain-size analysis of ancient deep-marine sediments using laser diffraction. *Front Earth Sci*. (2022) 10. doi: 10.3389/feart.2022.820866

51. Houghton JE, Behnsen J, Duller RA, Nichols TE. Worden RH. Particle size analysis: A comparison of laboratory-based techniques and their application to geoscience. *Sedimentary Geology*. (2024) 464:106607. doi: 10.1016/j.sedgeo.2024.106607

52. Qian N, Wan Z. Sediment mechanics. *Beijing: Sci Press*. (2003).

53. Zhang H, Wang J. Experimental study on the underwater angle of repose of sand and model sand. *J Sediment Res*. (1989) 03):90–6. doi: 10.16239/j.cnki.0468-155x.1989.03.012

54. Jin L, Shi X. A preliminary discussion on the underwater angle of repose of model sand. *J Sediment Res*. (1990) 03):87–93. doi: 10.16239/j.cnki.0468-155x.1990.03.012

55. Men Z, Yang W. Preliminary exploration of difference between submarine angle of reposeand internal friction angle of sediment particles. *J Sediment Res*. (2012) 04):76–80. doi: 10.16239/j.cnki.0468-155x.2012.04.011

56. Wu Z, Zhang G, Liang Z, Xu Q. Influence of particle shape and medium on sediment repose angle. *Yellow River*. (2017) 39:24–7.

57. Zhang R. River sediment dynamics. *Beijing: China Water&Power Press*. (1998).

58. Meng L, Wang L, Wang Q, Zhao J, Zhang G, Zhan C, et al. Geochemical characteristics of the modern yellow river delta sediments and their response to evolution of the sedimentary environment. *Front Mar Sci*. (2024) 11:1370336. doi: 10.3389/FMARS.2024.1370336